

Role of precursor chemistry on synthesis of Si–O–C and Si–O–C–N ceramics by polymer pyrolysis

S. Rangarajan · P. B. Aswath

Received: 18 January 2010/Accepted: 9 November 2010/Published online: 24 November 2010
© Springer Science+Business Media, LLC 2010

Abstract In this study, the role played by polymer precursor chemistry on the nature of the pyrolyzed product was examined. Variables examined included extent of conjugation of the precursor, differences between a homopolymer and co-polymer, linear and cyclic structures, siloxanes and silazanes and between vinyl and phenyl containing silanes. Results indicate increasing the vinyl content of the precursor increases the amount of free carbon in the pyrolyzed product. The introduction of an aryl group in the silane decreased yield and lastly there was no change in the yield when a silazane was used instead of a silane, however, the composition of the silazane precursor ceramic is rich in nitrogen while a silane precursor ceramic is rich in carbon.

Introduction

The processing of ceramics by pyrolysis of polymeric precursors holds tremendous potential because the route has been successfully utilized to make a variety of ceramics such as SiC, Si_3N_4 , AlN, BN, etc. [1–10]. This process was first demonstrated by Yajima et al. [1, 2] to make SiC and has been successfully produced in the form of fibers and marketed as NicalonTM fibers by Sumitomo Corporation. The principal advantages of using polymer pyrolysis over other conventional techniques like powder processing are: lower processing temperatures; ease of processing large complex shapes; better control of impurities and the potential for developing materials with tailored microstructures, e.g.,

composites [11, 12]. Some of the potential applications for these materials include, high strength and modulus fibers [1, 2], coatings for environmental protection, batteries [13], luminescence [14], polymer infiltration processing of composites [11, 15], etc. Apart from the aforementioned ceramics, this process has been utilized to make a variety of amorphous materials, like silicon carbonitride (Si–C–N) [16], silicon oxynitride (Si–O–N) [17], and silicon oxycarbide (Si–O–C) [18]. It has been reported that both the cationic and anionic substitution in SiO_2 leads to the significant improvement in mechanical properties like Young's modulus, hardness, strength, fracture toughness, etc. [18, 19]. Substitution of O with either trivalent N or tetravalent C is expected to increase the cross-linking and thereby tightening the structure and increasing density. In this respect, C is the preferred substituent due to the greater extent of cross-linking because of its four-fold coordination. Early attempts to make silicon oxycarbide involved mixing SiO_2 with carbon, subsequently, C was incorporated by melting SiO_2 along with SiC [20, 21]. However, only 2.5% C could be introduced using this technique. In order to realize the improvement in properties, not only should greater amounts of C be incorporated but it must also be introduced directly into the Si–O network and not as "free carbon". An alternative route to processing silicon oxycarbides is to use organosilicon compounds. The advantage of using such a route is that C is easily introduced into the network and Si–C bonds are established in this stage. These linkages are retained in the final ceramic obtained on pyrolysis. Most studies have concentrated on the sol–gel route where organically modified silicon alkoxides or chlorides are used as precursors [22–25]. In these precursors, the Si–C bonds are created by hydrolysis/condensation reactions, which are subsequently pyrolyzed into oxycarbide glasses. A variation of this process is more popular as polymer pyrolysis in which

S. Rangarajan · P. B. Aswath (✉)
Materials Science and Engineering Department, University of Texas at Arlington, P.O. Box 19031, Arlington, TX 76019, USA
e-mail: aswath@uta.edu

addition polymerization reactions are used to form the initial Si–C linkages [12, 17]. In a recent study with silazanes, it was shown that pyrolysis of tetraethyl and teracycle siloxane and trimethyl and trivinylcyclotrisilazne resulted in a composite with an amorphous Si–O–C–N matrix with nanocrystals of SiC embedded in them [26]. Interrante et al. [27] showed that by blending precursors it is possible to develop interesting new ceramic architectures. Other studies with fillers have shown that the extent of shrinkage and cracking maybe controlled by the use of active and inactive fillers [28, 29].

Advances have been made by utilizing gravimetric and spectroscopic techniques such as thermo gravimetric analysis [30–32], solid state MAS Nuclear Magnetic Resonance spectroscopy [33–36], FTIR, X-ray diffraction [26, 37], extended X-ray absorption fine structure (EXAFS), X-ray photoelectron spectroscopy (XPS) [11, 14], etc., to understand the conversion process from preceramic polymer to ceramic. In this study, the approach was to understand the pyrolysis process by studying the effect of preceramic polymer structure, composition, and architecture on the pyrolyzate using available techniques such as FTIR and XPS together with chemical analysis.

Experimental procedures

Materials and processes

The materials used for his study were, cyclic vinyl methyl siloxane ($n = 3\text{--}4$), cyclic methyl hydro siloxane ($n = 4\text{--}6$), poly methyl hydro siloxane, poly dimethyl siloxane copolymer, tetra methyl tetra vinyl cyclotetrasilazane, tri-vinyl methyl silane, and phenyl methyl vinyl silane. All of the above was obtained commercially and were >99% pure.

Curing

All precursor solutions were cured using addition polymerization reaction [38]. In this process, 0.5-wt% hydro-silylation reaction catalyst, platinum divinyl tetramethyl disiloxane complex was added. The solution was then cured by heating the solution to 100 °C in air for 10 h.

Pyrolysis

Cured polymer samples were pyrolyzed into ceramics by heating to 982 °C in an inert atmosphere. Samples (~1 g) were pyrolyzed in tube furnace by heating from 25 to 982 °C at 5 °C/min. Ultra high purity argon (99.9999%) at a 100 cc/min flow rate was used.

Thermogravimetric analysis

All thermo gravimetric analysis of the polymer precursors were conducted in a TA Instruments Model 2050 TGA at a heating rate of 5 °C/min in an environment of flowing nitrogen (99.99% purity) from room temperature to 600 °C for the precursors and up to 1000 °C for the pyrolysis study.

Characterization of the pyrolyzed product

Chemical analysis

Quantitative Technologies Inc, New Jersey, USA conducted C, H, and N analysis on the pyrolyzed samples to determine the chemical composition. The analysis was performed using optimum combustion techniques.

Fourier transform infrared (FTIR) spectroscopy

Fourier transform infrared (FTIR) spectroscopy was performed using a Biorad FTIR. Liquid samples were run in a KBr cell in the transmission mode. Cured samples were mixed and powdered along with KBr to obtain the spectrum in the diffuse reflectance mode.

X-ray photoelectron spectroscopy (XPS)

Pyrolyzed samples were cleaned with acetone using a cotton tip. This surface was then visually inspected under an optical microscope at $\times 500$ for a clean surface. The sample was ultrasonically cleaned with isopropyl alcohol to remove residual deposit followed by ultrasonic cleaning in distilled water. Finally, all traces of moisture and other volatiles were removed by heating in an oven at 105 °C. Monochromatic AlK α ($h\nu = 1486.6$ eV) radiation from a Perkin–Elmer spectrophotometer was used. Survey and high-resolution scans were performed at an analyzer angle of 70°. The high angle provides bulk information rather than just surface analysis. High-resolution scans of Si 2p, O 1s and C1s peaks were obtained to determine the chemical bond configurations and chemical composition of the pyrolyzed ceramic. The charging effect was prevented using a neutralizer (low energy electron gun). The binding energies (BE) reported were obtained by matching the graphitic peak at 284.3 eV.

Variables used in the synthesis of the silicon oxycarbide and silicon oxynitride glasses

In order to understand the role of processing variables on the structure and composition of the final ceramic, a test matrix was developed (see Table 1). The starting liquid precursors are identified in Table 2 and mixed to form

Table 1 Experimental variables examined in this study

Effect	Experimental variable
Effect of mixing ratios of precursor solution	Effect of varying H/Vi ratios in the starting precursor.
Homo versus co-polymer	Differences between the cure and pyrolysis of a homopolymer and co-polymer
Linear versus cyclic	A linear chain polymer is compared with a cyclic polysiloxane
Effect of nitrogen in the backbone	Siloxane is compared with a silazane
Effect of vinyl and phenyl functional silanes	Effect of vinyl and phenyl containing silanes

Table 2 Chemical names and structures of precursors used in the pyrolysis

Starting liquid ID	Chemical name of liquid	Structure
Liq I	Polymethyl hydro siloxane	
Liq II	Polydimethyl siloxane (67.5%) + polymethyl hydro siloxane (32.5%)	
Liq III	Methyl hydrocyclosiloxane ($n = 4-6$)	
Liq IV	Cyclic vinyl methyl siloxane ($n = 3-4$)	
Liq V	Tetra methyl tetra vinyl cyclo tetrasilazane	
Liq VI	Trivinyl methyl silane	
Liq VII	Phenyl methyl vinyl silane	

solutions whose compositions are given in Table 3. The approach adopted here was to systematically vary the structure and composition of the starting precursors.

Results

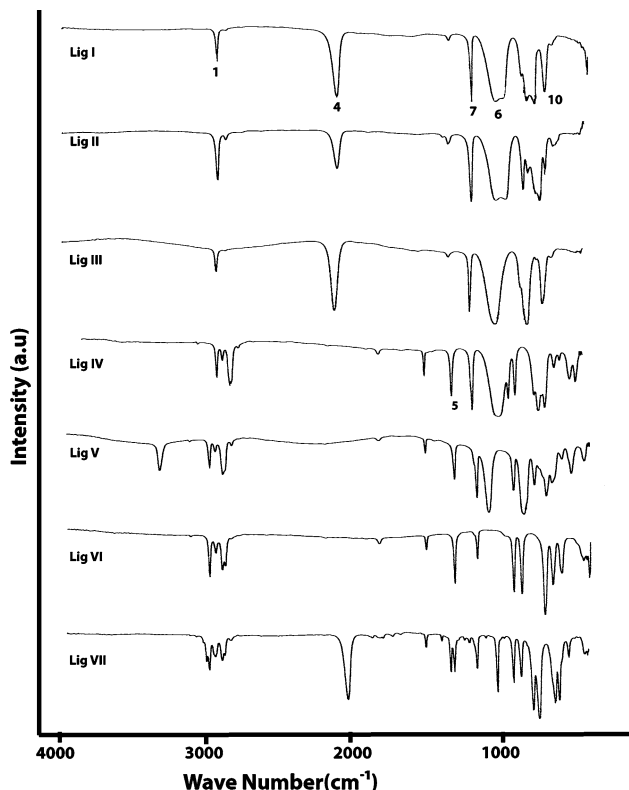
FTIR spectroscopy of liquid precursor samples

The FTIR spectra were obtained for all the liquid precursor samples and are presented in Fig. 1a–g. The sample identification and molecular structure are presented in Table 2. In order to clearly establish the transitions in the precursors, the liquid samples were analyzed completely and peaks were assigned. Table 4 lists the most frequently occurring vibrational modes and frequency range in which

they were observed. As can be seen from the figures, many overlapping peaks and peak shifts can be seen when the spectra are compared with each other. For ease of comprehension, the spectrum of Liq I in Fig. 1 is described in great detail. All subsequent spectra are interpreted with respect to this and only the differences and new peaks are identified and explained. Although it should be mentioned that successful identification of all peaks was not possible as is usually the case. The spectrum of Liq I is that of $(MeHSiO)_n$ with trimethyl silyl end groups. It should be mentioned here that this spectrum exactly reproduces that of $(MeHSiO)_x$ found in reference [39]. From the figure the two of the most intense bands at 2167 cm^{-1} for Si–H stretch and at $1000-1100\text{ cm}^{-1}$ for Si–O–Si asymmetrical stretch. The Si–O–Si stretch is split into two bands at 1094 and 1032 cm^{-1} . This is characteristic of polysiloxanes with

Table 3 Identification of polymer precursor solutions prepared for pyrolysis study

ID of mixture	Composition	H/Vi ratio	Comment
Sol I	1.44 Liq III + Liq IV	1.44	Mixing ratio and copolymer study
Sol II	Liq III + Liq IV	1	
Sol III	Liq III + 0.4 Liq IV	0.4	
Sol IV	1.44Liq I + Liq IV	1.44	Mixing ratio and copolymer study
Sol V	Liq I + Liq IV	1	
Sol VI	Liq I + 0.4 Liq IV	0.4	
Sol VII	Liq II + Liq IV	1	Linear versus cyclic
Sol VIII	Liq V +Liq IV	1	Comparison of silazane to siloxane
Sol IX	Liq VI + 3 Liq II	1	Vinyl silane: effect of vinyl silane versus linear siloxane
Sol X	50 wt% (Liq VII) + 50 wt% (Sol VII)	1	Phenyl silane: effect of vinyl and phenyl containing silane

**Fig. 1** IR spectra of samples Liq I through VII. Numbers indicate ID numbers corresponding to peaks in Table 4

$n > 4$ [40]. In addition, the δ_{as} SiCH₃ at 1261 cm⁻¹ and others (see Fig. 1) show the presence of the CH₃ group. The Si—C and Si—C₂ stretches are at 800 cm⁻¹ and 712 cm⁻¹, respectively.

The spectrum of Liq II in Fig. 1 which is a copolymer (see Table 2) is very similar to that of Liq I. The presence of the dimethyl group gives a more intense peak for Me group deformations. In addition, the γ -CH₃ peaks are split and two bands are seen at 760 cm⁻¹ and \sim 800 cm⁻¹. The ν Si—H peak shift from 2167 in homopolymer to 2159 in the copolymer, while the Si—H bending vibration occurs at 912 cm⁻¹.

The spectrum for Liq III is also shown in Fig. 1. Comparing with spectrum for Liq I, the differences are: (i) due to the absence of the terminal methyl groups, the peaks due to the Me groups are less intense, (ii) the Si—O—Si bands are not split which again is characteristic of cyclic structures.

Figure 1 also shows the spectrum for Liq IV ([MeVi-SiO]). Characteristic vibrations associated with the vinyl group can be easily identified. For example the C=C stretch occurs as a sharp band at 1597 cm⁻¹. Other frequencies associated with the vinyl group are identified in Fig. 1. The Si—O—Si stretch occurs at 1075 cm⁻¹, slightly lower than the value expected for cyclic structures (1080 cm⁻¹) which is possibly caused by steric effects. Liq IV is a mixture of cyclics with three and four members.

Comparing the spectrum in Fig. 1 of Liq V to that of Liq IV, the differences in introducing nitrogen into the backbone are: (i) N—H stretch at 3386 cm⁻¹, (ii) N—H bending at 1174 cm⁻¹, (iii) asymmetrical Si—N—Si stretch at 940 cm⁻¹, (iv) absence of Si—O—Si band at 1075 cm⁻¹, (v) Shift to higher frequencies of most vibrations associated with Me and Vi groups again possibly due to the lower strains in the nitrogen containing rings.

Figures for Liq VI and VII show the vinyl and phenyl containing silane spectra, respectively. Spectra for Liq VI in Fig. 1 show no anomalies and all Vi group frequencies and Me are observed. Spectra for Liq VII in Fig. 1 the characteristics frequencies of the Ph groups can be seen at 1540 cm⁻¹, 1490 cm⁻¹, 1428 cm⁻¹, and 1114 cm⁻¹. Heavy overlap of peaks prevents complete identification of the spectra.

Curing of precursor solutions

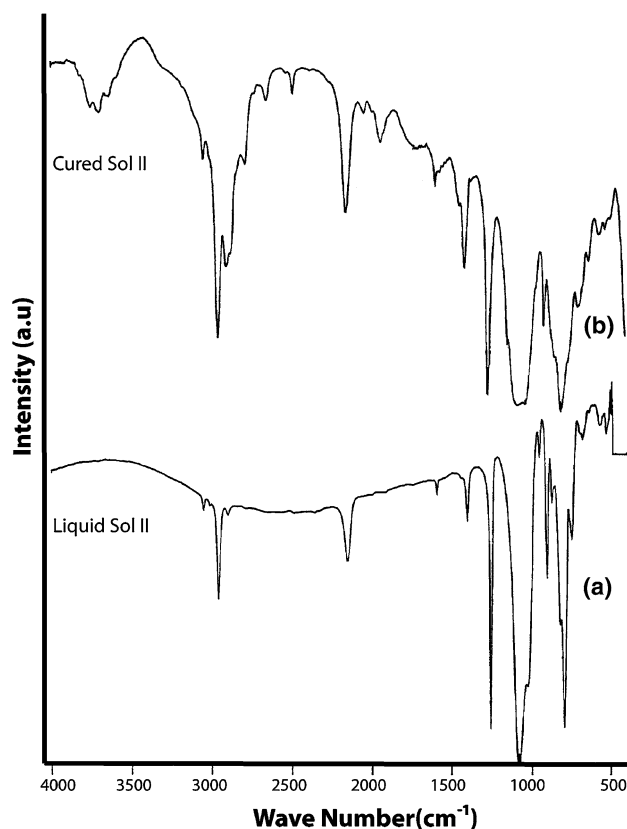
Solutions Sol I–Sol IX were mixed up in the ratios shown in Table 5 and cured. The cured product was characterized by FTIR spectroscopy. Figure 2a, b shows the spectra for liquid solution and cured Sol II, respectively. Many new

Table 4 Characteristic IR vibrations in the precursor polymers

Number	Group/bonds	Mode	Frequency range (cm^{-1})
1	$-\text{CH}_3$	ν_{as} (C–H)	≈ 2960
2	Alkane CH_2	ν_{as} (C–H)	≈ 2926
3	Alkane CH	ν_{as} (C–H)	≈ 2890
4	Si–H	ν_{as} (Si–H)	2157
5	Vinyl	ν_{as} (C=C)	1596
6	Si–O–Si	ν_{as} (Si–O–Si)	1000–1100
7	Si– CH_3	δ_{s} (Si–Me)	1261
8	Si–(CH_2) ₂ –Si	ω (CH_2 – CH_2)	1060
9	Si–(CH_2) _n –Si	δ (CH_2 – CH_2)	≈ 1600
10	Si–C	ν_{as} (Si–C)	796
11	Si–OH	δ (Si–OH)	830–950
12	$-\text{OH}$	ν (O–H)	≈ 3700

bands are seen on curing, which are attributed to the following:

- (i) The formation of Si– CH_2 – CH_2 –Si bonds due to the hydrosilylation reactions. This is confirmed by the appearance of band at 1137 cm^{-1} due to in-phase wagging of the two CH_2 groups. The out of phase wagging of the groups occurs with another sharp band at 1060 cm^{-1} . Unfortunately, this is not seen unless very intense, due to the interference from ν_{as} Si–O–Si. Also the appearance of C–H ($-\text{CH}_2-$) stretch and $-\text{CH}_2-$ scissors at 2910 cm^{-1} and 1442 cm^{-1} , respectively, confirm the presence of the Si– CH_2 – CH_2 –Si linkages.
- (ii) The appearance of peaks in the 3600 – 3800 cm^{-1} is attributed to the O–H stretch possibly due to the formation of Si–OH bonds. This could not be confirmed because the broad band arising from Si–O (Si–OH) stretching vibration in the range of 830 – 950 cm^{-1} is absent. This absence is probably

**Fig. 2** IR spectra of Sol II showing spectra of (a) liquid and (b) cured sample

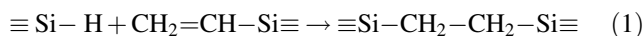
the result of several overlapping peaks in that region (see Fig. 2a).

- (iii) The appearance of other peaks may probably be due to combinations and overtones, sample contamination through adsorption of CO_2 species, etc. Although other reactions are possible, DSC scans on the liquid precursor solution show the appearance of a single peak attributable to the hydrosilylation reaction.

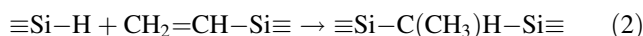
Table 5 Carbon composition of precursor and final ceramic

Sol. ID	Composition	Calculated %C in polymer	%C from CH_3	%C from Vinyl	H/Vi ratio in polymer	%C in ceramic	% ceramic yield
Sol I	Liq III + Liq V	32.5	26.5	6.0	1.44	11.0 ± 3	70.0
Sol II		33.3	25.4	7.9	1	25.2 ± 8	76.4
Sol III		35.8	21.9	13.9	0.4	25.9 ± 0.8	74
Sol IV	Liq I + Liq IV	30.8	16.6	14.2	1.44	17.8 ± 5.5	81.6
Sol V		32.7	16.1	16.7	1	20.1 ± 5.6	82.4
Sol VI		36.9	15.0	21.9	0.4	21.4 ± 2.8	79.1
Sol VII	Liq II + Liq IV	32.9	16.4	16.5	1	26.2 ± 3.5	82.5
Sol VIII	Liq V + Liq IV	34.0	17.0	17.0	1	27.4 ± 2.0	81.0
Sol IX	Liq II + Liq VI	37.5	15.0	22.5	1	25.4 ± 8.5	83.3
Sol X	Liq II + Liq IV + Liq VII	52.8	12.3	16.3	1	35.8 ± 4.3	54.9

Therefore the curing in the samples could be caused by the following reactions:

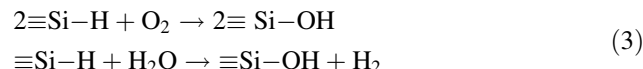


which is the hydrosilylation reaction. It should be noted here that the addition of Si to the olefin occurs according to Farmers rule [41] in which Si adds to the most hydrogenated carbon atom. Addition to the other carbon atoms is possible depending on steric effects and inductive effects of functional groups on the carbon. This reaction is represented in Eq. 2

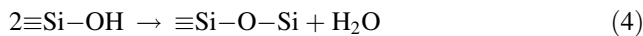


Evidence of this reaction is restricted to the appearance of alkane C–H stretch at $\sim 2890 \text{ cm}^{-1}$. Unfortunately, other peaks due to $\delta\text{-CH}_3$, Si–C–Si, etc., overlap with already existing peaks and hence cannot be confirmed by IR spectroscopy.

In addition to this, reaction of Si–H to form silanols is also possible through one of the possible mechanisms



Although the silicon hydride bonds are stable, the formation of silanol groups can be catalyzed by oxidative agents like platinum catalysts. The source for both O_2 and H_2O in the above reactions is the atmosphere, and pick-up of these is easily possible during curing which is performed in laboratory air environment. It has been reported [8, 18] that these silanols have a tendency to undergo condensation to form Si–O–Si linkages according to Eq. 4;



Curing of Sol I through Sol IX did not bring about many changes when compared with each other. The mechanisms of curing for all the solutions appear to be the same as mentioned above. Although it should be mentioned that curing is not complete in any of the cases as indicated by the bands due to vinyl and hydro group, which are still seen except in the case of Sol VIII. The Sol VIII shows the presence of only Si–H bonds which possibly occur due to evaporation of Liq VI (MeSi(Vi)_3) during the cure process. Comparing spectra of Sol I, Sol II, and Sol III, it can be seen that decreasing the H/Vi ratio increases the intensity of vinyl group frequencies (1597 cm^{-1}) and decreases those of hydro groups (2157 cm^{-1}). One common feature of the curing process is the shift of ν_{as} Si–O–Si to lower frequencies centering around $\sim 1060 \text{ cm}^{-1}$ which is attributed to the formation of Si–CH₂–CH₂–Si bridges which as mentioned previously has a sharp band at 1060 cm^{-1} . Another feature of the cure process is that in the case of cyclics, polymerization did not cause ring opening as indicated by ν_{as} Si–O–Si bands, which remained sharp and unsplit.

Pyrolysis

Summary of results obtained from the pyrolysis of cures samples is presented in Table 5. Ceramic yields on pyrolysis range from $\sim 55\%$ in Sol IX to 83% in Sol VIII. The Table also lists the results of chemical analysis on the samples. The results presented for percentage of carbon in the pyrolyzed ceramic represent average of triplicate analysis. It was found that percentage of C in the samples varied by large amounts as can be seen from the average deviation in the results. Two factors that could contribute to this are (a) heterogeneity of samples and (b) incomplete combustion. The exact cause for this anomaly is yet unknown.

Figure 3 shows a representative FTIR spectra of the pyrolyzed ceramic. The occurrence of two broad bands at 1014 and 809 cm^{-1} confirm the presence of Si–O and Si–C bonds. The presence of amorphous carbon is indicated by the broad peak at 1800 cm^{-1} . The ceramic structure was further analyzed using XPS. Figure 4 shows the results of the survey and high-resolution scans on the sample Sol VII. The XPS spectra was analyzed and interpreted, and compared with published data [42–44]. The deconvoluted C1s peak clearly shows the presence of carbon in the two major forms. The first peak at 284.3 eV represents carbon in graphitic/turbostratic form (free carbon). The second peak at 282.5 eV is associated C–Si bond in oxycarbide environment. The carbon peak for SiC is shifted to lower energies and is at 282.5 eV [45]. A third small peak can also be seen in the figure and is attributed to Si–C–O bonds. Table 6 shows summary of XPS results on all tested samples.

Table 6 also gives the chemical composition of the samples as calculated from high-resolution XPS scans and is compared to the experimental obtained values. It should be mentioned here that chemical information presented here is semi-quantitative and there is 5–10% associated error. This is especially true in heterogeneous samples because of different sensitivity factors for each element and different charging effects of different ceramic species. But

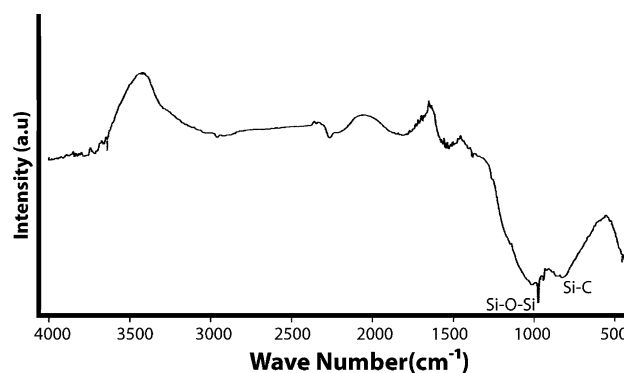


Fig. 3 Spectra of pyrolyzed sample of Sol II

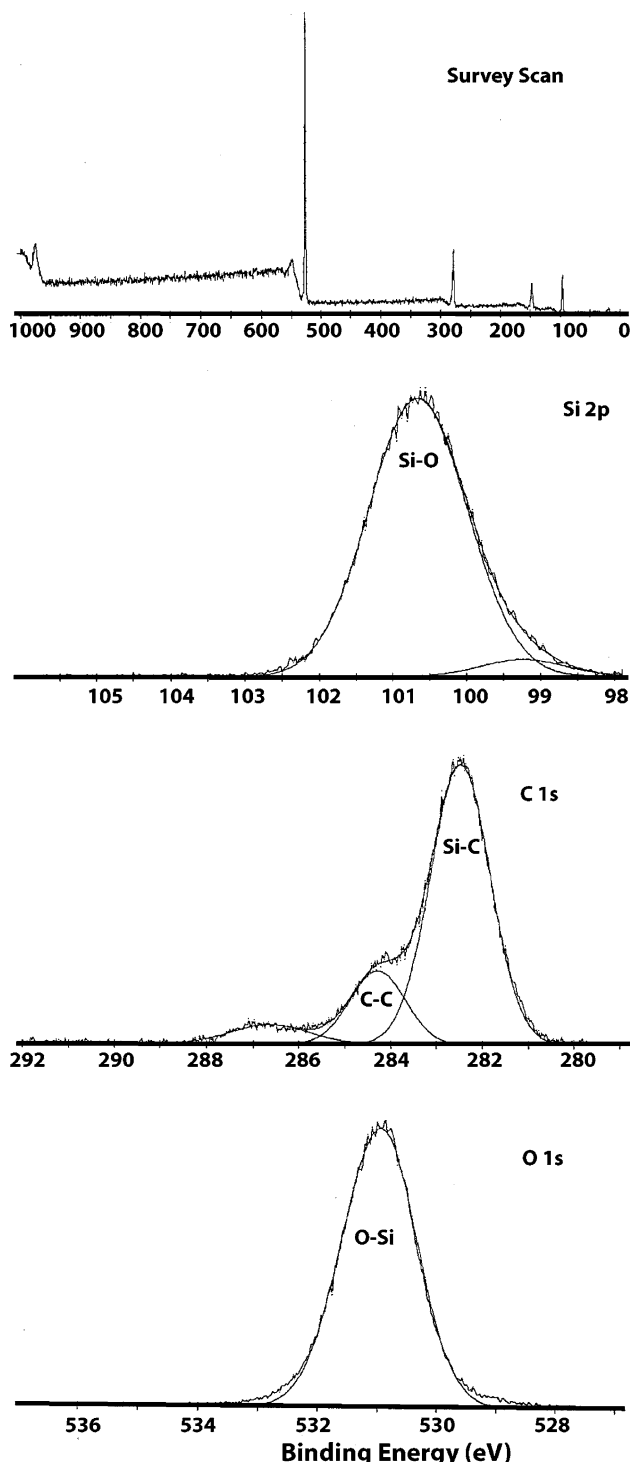


Fig. 4 XPS spectra of sample Sol VII showing survey and high-resolution scans. The Si_{2p}, C_{1s} and O_{1s} peaks are deconvoluted

despite this, XPS provides useful information regarding trends. From the results it is apparent that

- (i) Trends indicated in carbon concentration (obtained from chemical analysis) are approximately maintained in the XPS analysis.

- (ii) Oxygen content in the ceramic as shown by XPS analysis is very high.

Although the oxygen sensitivity is exaggerated possibly due to high sensitivity factor of oxygen (0.66 vs. 0.25 for C and Si) and as can be seen from the intensity of O_{1s} peak, the atomic concentration of oxygen can safely be taken to be higher than the precursor. The Si/O ratio for the ceramic increases from an initial value of 1 in the precursor. This implies that either Si is lost during pyrolysis or there is a gain in oxygen. The former hypothesis is unlikely as this would imply cleavage of Si–O bonds, which is stable and has not been reported in any of the earlier studies. Since the pyrolysis was conducted in an oxygen free environment, it seems likely that oxygen was picked up during the cure process. It was earlier indicated after examination of the IR spectra that this was possible by Eq. 3.

Comparison of results for Sol IV–Sol VI shows that with decrease in H/Vi ratio, the carbon concentration in the ceramic product increases. In addition, it can be seen that a high carbon concentration is retained in the ceramic when cyclic precursors are used (Sol VII and Sol VIII). The highest carbon content was found in Sol X with phenyl groups. When expressed as fraction of the initial carbon present, it is clearly evident that higher fractions of carbon are retained if cyclics are used. In addition, for H/Vi ratios close to one, greater cross-linking through formation of Si–CH₂–CH₂–Si bridges promote a greater retention of carbon. Also presented in Table 7, is the fraction of oxy-carbide and graphitic phases as calculated from the areas under the deconvoluted C_{1s} peaks. It is again seen that fractional amount of free carbon is reduced and oxycarbide increased when,

- (i) cyclics are used,
- (ii) H/Vi = 1,
- (iii) copolymer is used instead of homopolymer.

Although use of excess amount of vinyl groups increased carbon concentration in the ceramic, there is a greater tendency to form graphitic carbon rather than network carbon.

Discussion

Mechanisms of transformation

From the results, two clear trends are exhibited.

- (i) Yield is maximized when H/Vi ratios equal to 1 are used and also when cyclics are used.
- (ii) As the H/Vi ratio decreases, the amount of graphitic carbon in the ceramic increases.

Table 6 Summary of XPS results of the pyrolyzed ceramic

	Solution ID	XPS chemical analysis			Chemical (CHN) analysis %C	Fraction of carbon forms from XPS analysis
		%Si	%O	%C		
	Sol I	33.7	47.4	18.8	11.0 ± 3	71.5
	Sol II	32.2	45.7	22.1	25.2 ± 8	71.0
	Sol III	35.3	48.9	15.8	25.9 ± 0.8	67.9
	Sol IV	—	—	—	17.8 ± 5.5	—
	Sol V	—	—	—	20.1 ± 5.6	—
	Sol VI	34.7	47.5	17.8	21.4 ± 2.8	67.9
– Not analyzed for	Sol VII	31.2	45.9	22.8	26.2 ± 3.5	75.3
						18.0

Table 7 IR activity of select functional groups as a function of temperature

Temperature °C	Sol IV	Sol V	Sol VI
100 °C	Si–OH	Si–OH ← ^a Si–H ← Si–Vi →	Si–H ←
200 °C	Si–Vi ^b Si–C, (ρ Si–CH ₃ w.r.t. ν Si–C) ↑ ν OH ↓	Same as Sol IV	Si–Vi → Si–H ↓
400 °C	Si–H (≈ same) Si–Vi disappears Si–(CH ₂) _n –Si ↑ Peak at 1630 cm ^{−1} H ₂ O	Si–H almost disappears Si–Vi almost disappears Si–(CH ₂) _n –Si ↑ Peak at 1630 cm ^{−1} H ₂ O	Si–H disappears Si–Vi ↓ Si–(CH ₂) _n –Si ↑ Peak at 1630 cm ^{−1} H ₂ O
600 °C		Appearance of broad band between 800 and 1000 cm ^{−1} Si–H reappears ↑ Peak at 1630 cm ^{−1} H ₂ O	Appearance of broad band between 800 and 1000 cm ^{−1} Si–H reappears ↑ Peak at 1630 cm ^{−1} H ₂ O

^a →, ← Indicates direction of increase

^b ↑ Peak intensity increases, ↓ peak intensity decreases

In order to explain these trends, a pyrolysis study was performed on Sol IV, Sol V, and Sol VI. Pyrolysis of these samples was interrupted at intermediate temperatures and the pyrolyzate analyzed using IR. Choice of temperatures was based upon TGA analysis on sample Sol II. Figure 5 shows the TGA data for Sol II along with weight loss data for Sol V at different temperatures. Also presented is the first derivative curve for Sol II. Five regions can be identified based on slope changes.

- (i) Region I: 25–300 °C
- (ii) Region II: 300–460 °C
- (iii) Region III: 460 to ~620 °C
- (iv) Region IV: 580–800 °C
- (v) Region V: temperatures greater than 800 °C

Region I, in which weight loss occurs is followed by a small weight loss in Region II. There seems to be no clear distinction between the Regions III and IV since the slope gradually changes in these regions. Above 800 °C, the

weight loss is again minimal. The temperatures chosen for the study were at 200 °C (Region I), 400 °C (Region II), and 600 °C (Regions III and IV). Figures 6 and 7 represent the IR spectra at various temperatures for Sol II and Sol III. Summaries of the observations and trends are presented in Table 7.

At 400 °C, no major changes are seen in the spectra except for decreases in the Si–H/Si–Vi groups. At 400 °C, the Vi and Hydro groups are either completely absent or almost extinct. This is accompanied by an increase in the intensity of Si–CH₂–CH₂–Si at ~1430 cm^{−1}. At 600 °C, surprisingly Si–H bond attributes reappears while bond attributed to O–H and water (broad peak at 1630 cm^{−1}) either disappear or are nearly extinct. Studies on the organic to inorganic transition during pyrolysis suggest that the transformations occur via a radical mechanism [46]. Therefore, radicals are formed by thermally induced changes of bonds. Based on bond dissociation energies (at 25 °C), the stabilities of various bonds in increasing order as follows [45]:

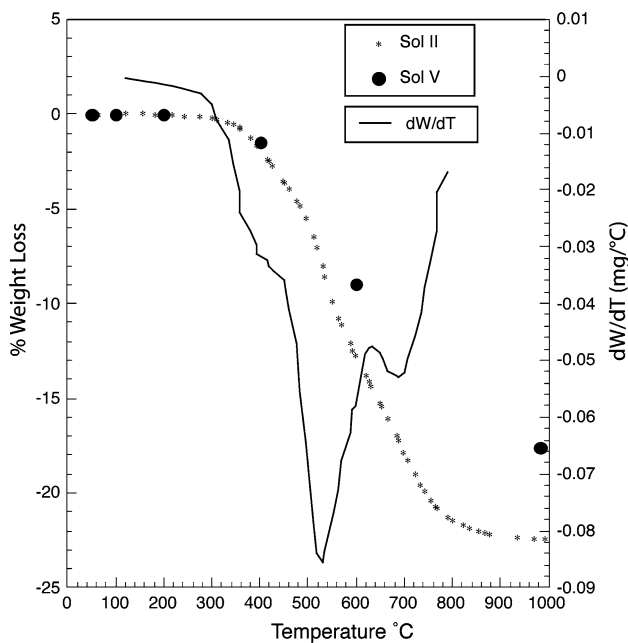


Fig. 5 Weight loss on pyrolysis plotted versus temperature. Two curves are plotted—curve for Sol II obtained from a TGA experiment while that for Sol V is the measured wt. change at intermediate temperatures. Also shown is the first derivative plot of the wt. loss for Sol II

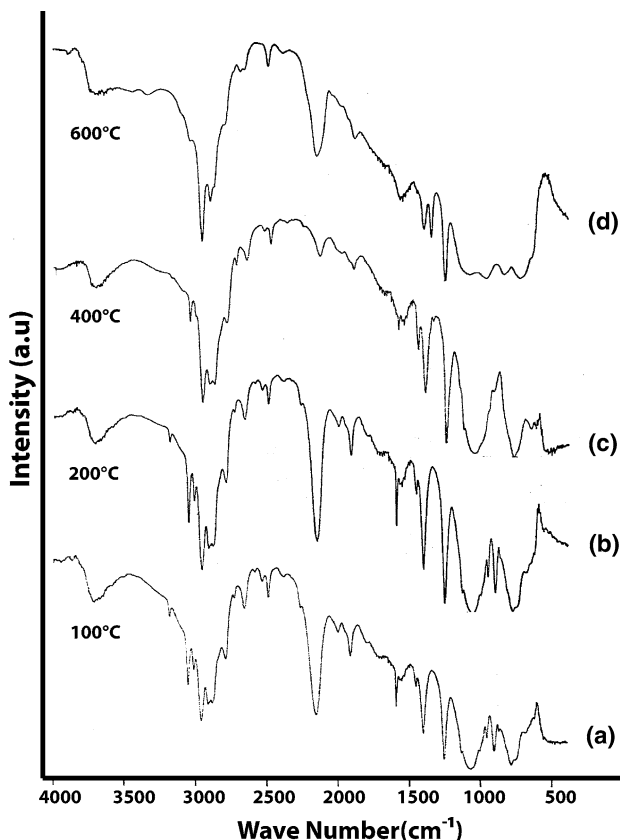
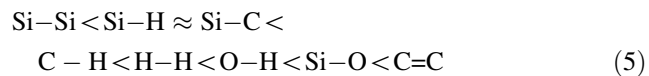


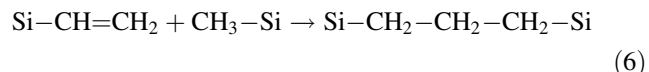
Fig. 6 IR spectra of sample Sol V after intermediate temperatures of pyrolysis to show transitions from polymer to ceramic state. (a) After cure (100 °C), (b) after 200 °C (c) after 400 °C, and (d) after 600 °C



This suggests that the breakage of the bonds should also proceed in that order during pyrolysis. However, the above, rather simplified picture is somewhat complicated by other factors, such as

- (i) Steric effect that causes straining of the bonds.
- (ii) Inductive effect of the neighboring atoms.
- (iii) The reactivity of the groups to each other.

For example, although bond energy of Si-C is much lower than Si-OH, there is an extreme tendency of silanols to condense according to Eq. 4. However, there is no corresponding increase in the intensity of Si-CH₂-CH₂-Si peak at 1137 cm⁻¹. Therefore, a second cross-linking mechanism is operative in which thermally activated addition of methyl groups to vinyl groups occurs through the reaction



The small weight loss at this stage is explained by removal of the condensation products (Eq. 3), formation of H₂ and/or removal of un-reacted monomer units as volatiles. At 600 °C, analysis of the IR spectra reveals the presence of a broad band in the region of 700-1100 cm⁻¹. Formation of free radicals along with redistribution of the structure brings about Si-O-C bonds in addition to the already existing Si-OH. Absorption at 1630 cm⁻¹ suggests the presence of water that is a condensation reaction product. The analysis of bond energies in conjunction with IR spectra enables classification of bands as¹

Unstable : Si-H, Si-Vi, C-H

Stable : Si-(CH₂)_n-Si, Si-CH₂, Si-O-Si, Si-OH

Since Si-H vibrations reappears strongly, it is suspected that formation of the $\equiv\text{Si}^\bullet$ followed by H abstraction as elucidated in [47] is the cause of this. Examination of Figs. 6 and 7 in conjunction with Table 7 shows two possible sources of $\equiv\text{Si}^\bullet$ radicals. The decrease in the intensity of the peaks at 1410 and 1596 cm⁻¹ shows the instability of the vinyl groups. Although the band at 1410 cm⁻¹ also corresponds to δ_s Si-CH₃, the strong appearance of δ_{as} S-CH₃ at 1261 cm⁻¹ shows stability of CH₃ groups. Another possible source, is the Si-OH bonds, which is indicated by the decrease in intensity of the silanol vibrations.

¹ Unless in contact with another Si-OH whereby condensation occurs.

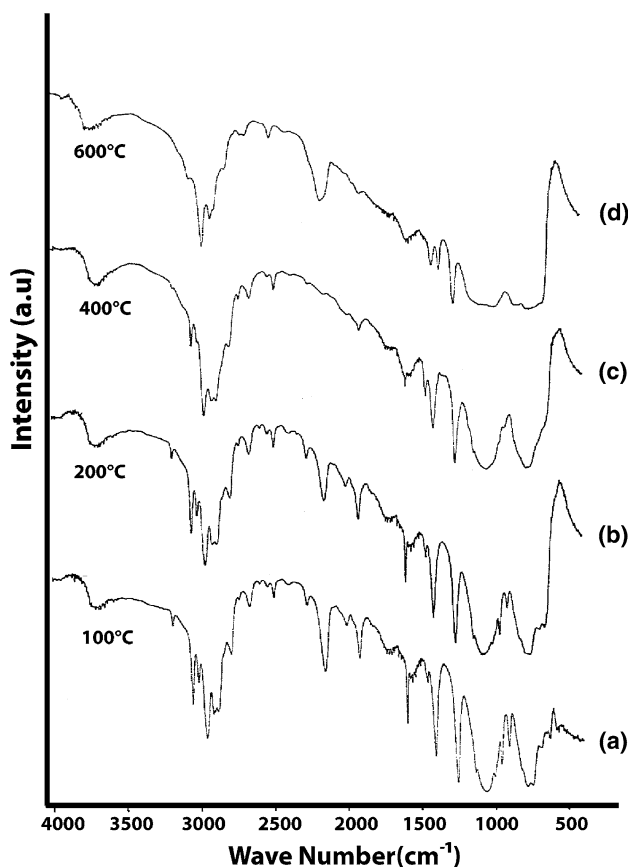


Fig. 7 IR spectra of sample Sol VI after intermediate temperatures of pyrolysis to show transitions from polymer to ceramic state. (a) After cure (100 °C), (b) after 200 °C, (c) after 400 °C, and (d) after 600 °C

Effect of variables on ceramic yield, structure, and composition

On comparison of results from Sol I to Sol VI a clear picture can be found. Comparing Sol I–Sol III to Sol IV–Sol VI, we find that the effect of the copolymer (poly methylhydrosiloxane or methyl hydrosiloxane) is only to change the yield and does not affect the extent of graphitic carbon. Therefore, the presence of larger amount Si–CH₃ group results in lower yields but does not contribute significantly to free carbon. The reason the yield is lower in the case of Sol I–Sol III is explained by the following mechanism. Earlier studies on the pyrolysis of poly dimethyl siloxane (PDMS) show that on pyrolysis PDMS forms D3–D7 cyclo siloxanes [40]. The structure consists of polycyclic siloxane “cages” which are interconnected. On further heating them the links break and siloxane units escape as volatiles. Therefore, loss of heavier siloxane species is directly responsible for decreased yield. This also explains drop in yield from Sol II to Sol I (76% → 70%). In comparison Sol V to Sol IV drop is just from 82% to

81%. Higher fraction of PDMS in Sol I is detrimental in overall yield of the pyrolysis process.

The formation of free carbon increases with increase in vinyl content. A explanation based on the IR and XPS results is now possible. Thermally activated curing of vinyl groups lead to the formation of Si–CH₂–CH₂–CH₂–Si bridges. With increase in vinyl groups more such bridges are formed. Driven by greater stability of the C–C bonds as compared to Si–C bonds, it is postulated that -(CH₂)_n–bridges cleave and form graphitic carbon. The presence of such a carbon phase helps in “binding up” the oxycarbide grains.

Retention of carbon in the ceramic has been shown to be directly influenced by cross-linking through hydrosilylation. In addition, this carbon is directly introduced into the reticulated network. Finally, when cyclics are used, more 3D cross-linking occurs during hydrosilation (as compared to linear siloxanes) thereby resulting in Si–CH₂–CH₂–Si or ≡ Si–CH(CH₃)–Si≡. ≡ Si–CH(CH₃)–Si ≡ is more stable compared to Si–CH₂–CH₂–Si. Therefore yield, which is a function of the carbon retained is maximum for H/Vi = 1 and in the case of cyclic structures.

The introduction of N in the precursor chemistry as in silazanes resulted in the incorporation of N in the pyrolyzed product in the form of Si–O–N and Si–O–C–N linkages. However, when nitrogen is used as a pyrolysis medium there is little incorporation of nitrogen in the structure of the finished product as gaseous nitrogen is very stable and does not crack to yield nitrogen radicals. On the other hand an earlier study [11] has shown that pyrolysis in NH₃ is very reactive and can incorporate N into the pyrolyzed product.

Conclusions

The following conclusions can be drawn from the research study:

1. Ceramic yield is maximized for H/Vi ratios close to 1. In addition, the carbon retention in the ceramic is maximized for this ratio.
2. Increasing the vinyl content increases the amount of free carbon in the ceramic.
3. The phenyl silane containing solution was markedly different from others. Aryl groups decrease the yield drastically.
4. Introduction of N in the backbone did not influence the yield but did significantly increase the amount of N in the pyrolyzed product.

Acknowledgements Support provided by the Materials Science and Engineering Department at University of Texas at Arlington is

gratefully acknowledged. Assistance provided by Dr. Xin Chen in acquiring the thermogravimetric data of the precursors is greatly appreciated.

References

1. Hasegawa Y, Iimura M, Yajima S (1980) *J Mater Sci* 15:720. doi:[10.1007/BF00551739](https://doi.org/10.1007/BF00551739)
2. Yajima S, Hasegawa Y, Hayashi J et al (1978) *J Mater Sci* 13:2569. doi:[10.1007/BF02402743](https://doi.org/10.1007/BF02402743)
3. Schmidt WR, Sukumar V, Hurley WJ Jr et al (1990) *J Am Ceram Soc* 73:2412
4. Schmidt WR, Interrante LV, Doremus RH et al (1991) *Chem Mater* 3:257
5. Legrow GE, Lim TF, Lipowitz J et al (1987) *Am Ceram Soc Bull* 66:363
6. Seibold MM, Russel C (1989) *J Am Ceram Soc* 72:1503
7. Seyferth D, Plenio H (1990) *J Am Ceram Soc* 73:2131
8. Hurwitz FI, Heimann P, Farmer SC et al (1993) *J Mater Sci* 28:6622. doi:[10.1007/BF00356406](https://doi.org/10.1007/BF00356406)
9. Erny T, Seibold MM, Jarchow O et al (1993) *J Am Ceram Soc* 76:207
10. Boury B, Corriu RJP, Douglas WE (1991) *Chem Mater* 3:487
11. Rangarajan S, Belardinelli R, Aswath PB (1999) *J Mater Sci* 34:515. doi:[10.1023/A:1004590527954](https://doi.org/10.1023/A:1004590527954)
12. Yu SH, Rimann RE, Danforth L, Leung RY (1995) *J Am Ceram Soc* 144:2410
13. Xing W, Wilson AM, Eguchi E et al (1997) *J Electrochem Soc* 144:2410
14. Karakuscu A, Guider R, Pavesi L et al (2009) *J Am Ceram Soc* 92:2969
15. Nejhad MNG, Bayliss JK, Yousefpour A (2001) *J Compos Mater* 35:2239
16. Moaer D, Pailler R, Naslain R et al (1993) *J Mater Sci* 28:2615. doi:[10.1007/BF00356196](https://doi.org/10.1007/BF00356196)
17. Leung RY, Gonczy ST, Shaun MS (1994) 07/816,269
18. Babonneau F, Bois L, Yang CY et al (1994) *Chem Mater* 6:51
19. Soraru GD, Liu Q, Interrante LV et al (1998) *Chem Mater* 12: 4054
20. Homeny J, Risbud SH (1985) *Mater Lett* 3:432
21. Homeny J, Nelson GG, Risbud SH (1988) *J Am Ceram Soc* 71:386
22. Belot V, Corriu RJP, Leclercq D et al (1992) *J Non-Cryst Solids* 144:287
23. Babonneau F, Bois L, Livage L (1992) *J Non-Cryst Solids* 147–148:280
24. Pantano CG, Singh AK, Zhang HX (1999) *J Sol-Gel Sci Technol* 14:7
25. Hurwitz FI, Farmer SC, Terepka FM et al (1991) *J Mater Sci* 26:1247. doi:[10.1007/BF00544462](https://doi.org/10.1007/BF00544462)
26. Schiavon MA, Ciuffi KJ, Valria I et al (2007) *J Non-Cryst Solids* 353:2280
27. Interrante LV, Moraes K, Liu Q et al (2002) *Pure Appl Chem* 74:2111
28. Greil P (2000) *Adv Eng Mater* 2:339
29. Greil P (1998) *J Eur Cer Soc* 18:1905
30. Campostrini R, D'Andrea G, Carturan G et al (1996) *J Mater Chem* 6:585
31. Dire S, Campostrini R, Ceccato R (1998) *Chem Mater* 10:268
32. Soraru GD, Pederiva L, Latournerie J et al (2002) *J Am Ceram Soc* 85:2181
33. Plawsky JL, Wang F, Gill WN (2002) *Am Inst Chem Eng J* 48:2315
34. Wang F, Gill WN, Kirk CA et al (2000) *J Non-Cryst Solids* 275:210
35. Radovanovic E, Gozzi MF, Goncalves MC et al (1999) *J Non-Cryst Solids* 248:37
36. Hurwitz FI, Meador MAB (1999) *J Sol-Gel Sci Technol* 14:75
37. Dire S, Ceccato R, Babonneau F (2005) *J Sol-Gel Sci Technol* 34:53
38. Blum YD, Laine RM (1992) *Abstr Pap Am Chem Soc* 203:36
39. Anderson DR (1975) In: Lee A (ed) *Chemical analysis*, vol 41. Wiley, New York, NY
40. Voronkov MG (1998) *Main Group Chem* 2:235
41. Shieh YT, Sawan SP (1995) *J Appl Polym Sci* 58:2013
42. Bouillon E, Pailler R, Naslan R et al (1991) *Chem Mater* 3:356
43. Porte L, Sartre A (1989) *J Mater Sci* 24:271. doi:[10.1007/BF00660966](https://doi.org/10.1007/BF00660966)
44. Laffon C, Flank AM, Lagarde P et al (1989) *J Mater Sci* 24:1503. doi:[10.1007/BF02397093](https://doi.org/10.1007/BF02397093)
45. Fritz G, Matern E (1986) *Carbosilanes: synthesis and reactions*. Springer-Verlag, New York, NY
46. Laine RM, Babonneau F (1993) *Chem Mater* 5:260
47. Bois L, Maquet J, Babonneau F et al (1994) *Chem Mater* 6:796